Rapid Communications

Meta-GGA performance in solids at almost GGA cost

Daniel Mejía-Rodríguez [*] and S. B. Trickey [†]

Center for Molecular Magnetic Quantum Materials, Quantum Theory Project, Department of Physics, University of Florida, Gainesville, Florida 32611, USA

(Received 27 August 2020; accepted 14 September 2020; published 29 September 2020)

A recent modification, r^{2}SCAN, of the strongly constrained and appropriately normed (SCAN) meta-generalized gradient approximation (GGA) exchange-correlation functional mostly eliminates numerical instabilities and attendant integration grid sensitivities exhibited by SCAN. Here, we show that the successful deorbitalization of SCAN to SCAN-L (SCAN with density Laplacian dependence) carries over directly to yield r^{2}SCAN-L. A major benefit is that the high iteration counts that hindered the use of SCAN-L are eliminated in r^{2}SCAN-L. It therefore is a computationally much faster meta-GGA than its orbital-dependent antecedent. Validation data for molecular heats of formation, bond lengths, and vibration frequencies (G3/99X, T96-R, and T82-F test sets, respectively) and on lattice constants, and cohesive energies (for 55 solids) and bulk moduli (for 40 solids) are provided. In addition, we show that the overmagnetization of bcc Fe, hcp Co, and fcc Ni persists in r^{2}SCAN but does not appear in r^{2}SCAN-L. Distinct from SCAN, both r^{2}SCAN and r^{2}SCAN-L give the correct nonmagnetic ground state for bcc V.

DOI: 10.1103/PhysRevB.102.121109

Setting and motivation. Recognition of chemically significant electron density inhomogeneities by use of an indicator function (usually denoted α; see below) is the critical mechanism by which a meta-GGA exchange-correlation (XC) functional improves upon a generalized gradient approximation (GGA). The most successful meta-GGA so far (see Ref. [1] and references therein), is SCAN, the strongly constrained and appropriately normed functional [2,3]. Its success is attributed to enforcement upon it of all known rigorous constraints which a meta-GGA can meet, together with calibration to the energies of certain primitive physical systems (the "appropriate norms"; see the Supplemental Material of Ref. [2]).

Despite its successes, SCAN introduced a numerical problem and exacerbated a methodological challenge [4–7]. We defer discussion of the methodological issue briefly. The numerical problem has two elements. SCAN exhibits high sensitivity to numerical integration grid density. Handling that requires extremely dense, hence costly, grids. The other element is instability of self-consistent field convergence that is hard to foresee, hence control, for a given system (especially in periodic solids).

Those two numerical issues with SCAN were addressed by Bartók and Yates [6] by a simple renormalization of the denominator of α, a rescaling of it, and replacement of the SCAN switching function $f(\alpha)$ with a smoother seventh-degree polynomial for $\alpha < 2.5$. The resulting revised SCAN (rSCAN) is far better behaved computationally than SCAN. rSCAN preserves both the good molecular bond lengths and vibrational frequency performance of SCAN. Unfortunately, rSCAN does not preserve the good performance of SCAN for benchmark molecular heats of formation [7]. In periodic solids, SCAN and rSCAN are about the same for lattice constants and cohesive energies [7] on a 55 solid test set [8] and for bulk moduli on a 44 solid set [9].

Very recently, Furness *et al.* [10] have shown that the shortcomings of rSCAN stem from the fact that its regularization resulted in the violation of several constraints satisfied by SCAN. They adopted the smooth switching function strategy of rSCAN combined with modifications to restore compliance with all but one of the constraints satisfied in SCAN. The result, their regularized-restored SCAN functional or r^{2}SCAN, recovers the strong performance trends of SCAN relative to molecular and solid data sets while maintaining the numerical stability of rSCAN.

The r^{2}SCAN combination of accuracy and stability opens an opportunity for an equally improved response to the methodological challenge. That comes from the regularized chemical region detector

$$\alpha(\mathbf{r}) := \frac{\tau_s - \tau_W}{\tau_{\rm TF} + \eta\tau_W}. \tag{1}$$

Here, $\tau_s = (1/2)\sum f_j|\nabla\varphi_j(\mathbf{r})|^2$ is the positive-definite Kohn-Sham (KS) kinetic energy density in terms of the KS orbitals φ_j and occupations f_j, τ_W and $\tau_{\rm TF}$ are the von Weizsäcker and Thomas-Fermi kinetic energy densities, respectively, and $\eta = 10^{-3}$ is a small regularization parameter. The original α has $\eta = 0$. Obviously the orbital dependence of the XC energy introduced by α disqualifies SCAN or r^{2}SCAN from being used in orbital-free density functional theory (DFT). Worse, that orbital dependence makes an ordinary KS calculation [11] almost prohibitively costly because it necessitates an optimized effective potential (OEP) calculation [12–15] at every self-consistent field (SCF) step. Usual practice to evade that cost is to do generalized-KS (gKS) calculations [16,17]. The gKS Euler equation follows from

[*] dmejiarodriguez@ufl.edu
[†] trickey@qtp.ufl.edu

TABLE I. Performance of SCAN, SCAN-L, r^{2}SCAN, and r^{2}SCAN-L for heats of formation (kcal/mol), bond lengths (Å), and vibrational frequencies (cm^{-1}) at various grid densities. Mean absolute errors with respect to experiment from the NWCHEM HUGE grid calculations are in boldface. For the lower-density grids, the mean absolute deviation and maximum absolute deviation (in parentheses), with respect to those HUGE results are shown.

	SCAN		SCAN-L		r^{2}SCAN		r^{2}SCAN-L	
Heats of formation	**4.93**		**5.66**		**4.49**		**5.30**	
`Coarse`	5.92	(26.61)	5.12	(22.02)	0.40	(1.80)	0.81	(5.90)
`Medium`	2.31	(15.56)	2.36	(14.63)	0.09	(0.54)	0.22	(1.19)
`Fine`	0.73	(4.25)	0.88	(4.59)	0.01	(0.09)	0.04	(0.22)
`Xfine`	0.23	(1.42)	0.36	(1.90)	0.00	(0.02)	0.01	(0.07)
Bond lengths	**0.009**		**0.011**		**0.010**		**0.011**	
`Coarse`	0.001	(0.016)	0.001	(0.014)	0.000	(0.003)	0.001	(0.006)
`Medium`	0.001	(0.006)	0.001	(0.006)	0.000	(0.002)	0.000	(0.001)
`Fine`	0.000	(0.004)	0.000	(0.004)	0.000	(0.000)	0.000	(0.001)
`Xfine`	0.000	(0.004)	0.000	(0.003)	0.000	(0.000)	0.000	(0.001)
Vib. frequencies	**31.1**		**28.8**		**30.9**		**25.6**	
`Coarse`	24.2	(150.5)	24.1	(183.0)	7.5	(71.2)	7.0	(55.9)
`Medium`	18.4	(330.2)	21.7	(156.4)	2.1	(21.1)	2.1	(22.0)
`Fine`	10.5	(100.0)	14.8	(130.5)	1.3	(11.6)	1.4	(12.9)
`Xfine`	3.6	(32.1)	5.1	(39.9)	0.5	(3.9)	0.6	(4.2)

the variation of the density functional approximation (DFA) with respect to the orbitals, not the density. For meta-GGA and higher-rung functionals the KS and gKS equations are not equivalent [18,19].

We addressed this challenge by deorbitalization [20–22]. The deorbitalized version of SCAN, SCAN-L, differs from SCAN only in using an orbital-independent approximation for τ_s in the original α to give $\alpha_L[n, \nabla n, \nabla^2 n]$ (with n the electron number density). The approximate τ_S is a reparametrization of the Perdew and Constantin kinetic energy density approximation [23]. As such, it has proper uniform coordinate scaling. The approximate α_L is just the Pauli enhancement factor of orbital-free DFT, hence it is properly dimensionless. Deorbitalization restores use of the KS equation. Furthermore, a SCAN-L calculation should be much faster than SCAN. In practice that advantage often went unrealized because numerical instabilities caused very slow SCF convergence. Experience [24] suggested that the problem might be rooted in the $\nabla^2 n$ dependence. By deorbitalizing r^{2}SCAN into r^{2}SCAN-L, we show here that much of the problem actually was inherited from SCAN.

Procedure and results. The deorbitalization of r^{2}SCAN used precisely the same deorbitalized τ_s form and parametrization as was used for SCAN-L in Refs. [20,21]. Molecular calculations were done with a locally modified developers' version of the NWCHEM code [25]. Similarly, the periodic solid calculations were done with a locally modified version of VASP 5.4.4 [26,27]. Note the remarks about coding in the VASP meta-GGA trunk in Ref. [21]. As in that reference, we did calculations with coding implemented in that trunk (to check unambiguously against the VASP results of Ref. [10]) and coding in the GGA trunk (to ascertain optimal speedup from the deorbitalization). Basis sets, cutoffs, and other matters of technique were as documented in Refs. [20,21] with one exception, the projector augmented waves (PAWs), documented below.

Table I summarizes the results for the molecular test sets in the form of mean absolute errors (MAEs) with respect to experiment for heats of formation (G3/99X set [28]), bond lengths (T96-R set [29]), and harmonic vibrational frequencies (T82-F set [29]) obtained with the NWCHEM HUGE grid. For lower-density grids, Table I shows the mean absolute deviation (MAD) and maximum absolute deviation (MAX) with respect to the HUGE grid results.

Table I confirms the necessity of very dense numerical integration grids for both SCAN and SCAN-L. Even the XFINE preset grid yields deviations above 1 kcal/mol and 30 cm^{-1} (bond lengths are less problematic). In contrast, r^{2}SCAN and r^{2}SCAN-L results are well converged with the MEDIUM and FINE grid presets. This is a major improvement both in reliability as well as in performance, since numerical integration easily can become a computational bottleneck. See below regarding the calculation of $\nabla^2 n$ on the integration grid in the context of a Gaussian-type orbital (GTO) basis.

It is important to note the disentanglement of instabilities due to the functional form versus the Laplacian dependence. It now is clear that SCAN-L exhibits roughly the same stability difficulties as SCAN because of their common structure. However, the highly stable r^{2}SCAN-L shows MAX thermochemical deviations (values in parentheses in Table I) about three times larger than those for r^{2}SCAN on a given preset grid. This residual grid sensitivity seems directly attributable to the Laplacian dependence of r^{2}SCAN-L and is comparable to that of a numerically sensitive GGA (see the Supplemental Material of Ref. [7]).

Different from the setup described in Ref. [21], the periodic solid calculations in VASP used the "no-suffix" PAW data sets instead of the GW ones. (Discussion of this choice is given below.) Since the PAW data sets used here are softer than the GW sets, we lowered the kinetic energy cutoff to 600 eV. The k-point sampling density was increased to match that reported in Ref. [10] by using the KSPACING=0.1 keyword.

TABLE II. Mean absolute error comparison for SCAN, SCAN-L, r^{2}SCAN, and r^{2}SCAN-L XC functionals for the solid state test sets.

	SCAN	SCAN-L	r^{2}SCAN	r^{2}SCAN-L
a_0 (Å)	0.034	0.038	0.037	0.039
B_0 (GPa)	7.4	8.8	6.0	8.9
E_{coh} (eV/atom)	0.21	0.21	0.20	0.33

TABLE III. Saturation magnetizations (μ_B/atom) of four elemental solids at their respective experimental lattice constants.

	bcc Fe	hcp Co	fcc Ni	bcc V
SCAN	2.60	1.80	0.78	0.57
SCAN-L	2.05	1.63	0.67	0.00
r^{2}SCAN	2.63	1.77	0.74	0.03
r^{2}SCAN-L	2.27	1.67	0.69	0.06

Table II shows MAEs with respect to experimental results for three crystalline test sets [21]: 55 equilibrium lattice constants (with cubic or hexagonal symmetry), 40 bulk moduli (cubic symmetry), and 55 cohesive energies. Zero-point effects were removed from experimental lattice parameters and bulk moduli.

Similar to the molecular case, Table II shows that deorbitalization of r^{2}SCAN is achieved with the same success as with SCAN. (Note that the values in that table are not directly comparable with our previous reports [7,21] because of the PAW data-set change.) In both cases, the lattice parameters are well treated. Predictions of bulk moduli and cohesive energies with both deorbitalized functionals show large percentage deviations, but the deviation magnitudes are nonetheless quite small (large percentage error in a small quantity). Some physics also is involved. Part of the cohesive energy MAE difference between r^{2}SCAN-L and r^{2}SCAN comes from the different electronic configurations found for the W atom. r^{2}SCAN-L, SCAN, and SCAN-L all find a $6s^1 5d^5$ valence when the configuration is unconstrained, while r^{2}SCAN finds the correct $6s^2 5d^4$ configuration.

The total time needed to converge the 660 single-point calculations (12 per each solid) was used as a surrogate measure of the speed and stability of each functional. Consistent with expectations, the total times relative to the SCAN benchmark were 0.924 for r^{2}SCAN, 0.438 for SCAN-L, 0.272 for r^{2}SCAN-L, and 0.227 for the Perdew-Burke-Ernzerhof functional (PBE) [30]. In other words, r^{2}SCAN-L computational cost in a plane-wave basis is almost as inexpensive as a standard GGA functional, even though numerical demands associated with the Laplacian dependence remain.

There is an important caveat. The SCF stability of all the approximate functionals, as measured by the number of iterations needed for convergence, can be degraded by use of the GW PAW data sets. The Laplacian-dependent functionals are significantly worse in this regard than the orbital-dependent ones. What one sees with some, but not all, of the GW data sets is erratic SCF convergence. In those cases, near SCF convergence from iteration steps $N-1$ to N often is followed by drastic worsening at step $N+1$. Exploration of the origins of this behavior is outside the scope of the present work.

Despite the fact that SCAN-L inherits many properties from SCAN, SCAN-L avoids the overmagnetization of simple elemental solids such as bcc Fe, hcp Co, fcc Ni, and bcc V [31]. We therefore tested r^{2}SCAN and r^{2}SCAN-L in those elemental solids at their respective experimental lattice constants (2.86, 2.50, 3.52, and 3.03 Å, respectively).

Table III shows that r^{2}SCAN predicts larger-than-expected magnetic moments for bcc Fe, hcp Co, and fcc Ni. Interestingly, r^{2}SCAN gives bcc V essentially as nonmagnetic, in sharp contrast to the SCAN prediction. On the other hand, r^{2}SCAN-L gives magnetic moments slightly larger than SCAN-L but still in the range that would be expected for an ordinary GGA functional. Moreover, r^{2}SCAN-L corrects the slight undermagnetization obtained with SCAN-L in bcc Fe.

An important theoretical aspect of the deorbitalization procedure is that it may modify the effects of a certain constraint satisfaction in the parent DFA without modifying the constraint itself. A clear example is that in some systems the spatial regions where $\alpha = 0$ and $\alpha_L = 0$ are not exactly the same. In one-electron systems, the consequence is that the deorbitalized functional no longer is *exactly* self-interaction free. The difference is small and has proven to be rather inconsequential. For example, the dissociation curves of the H_2^+ molecular cation, widely used as a measure of one-electron self-interaction error, are the same for SCAN, SCAN-L, r^{2}SCAN, and r^{2}SCAN-L. See Fig. 1.

Summary. The slow (sometimes extremely so) SCF convergence and numerical sensitivities of SCAN-L originate mostly in the structural characteristics of SCAN. The removal of those provided by r^{2}SCAN leads to a similarly well-behaved

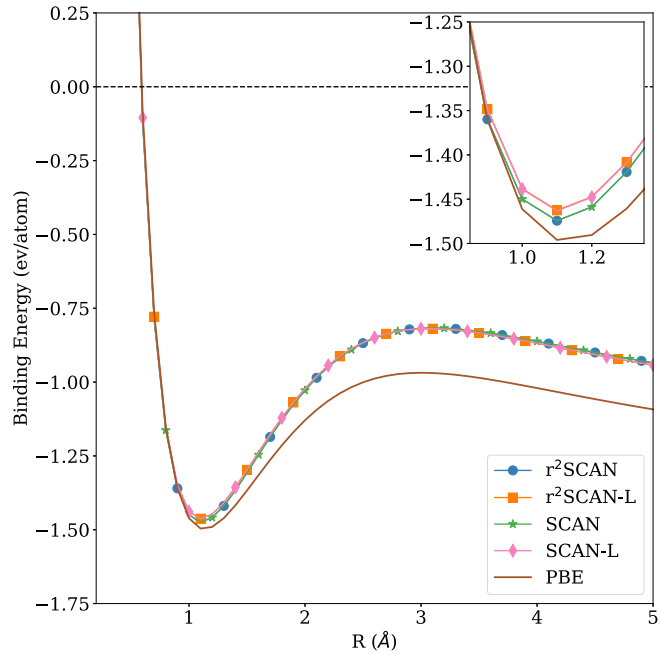

FIG. 1. Dissociation energy curves for the H_2^+ molecular cation as a measure of the one-electron self-interaction error. The inset zooms in on the well region.

deorbitalized version, r^{2}SCAN-L. Except for the elemental 3*d* solid magnetization discrepancy, r^{2}SCAN-L replicates the behavior of r^{2}SCAN on major molecular and solid benchmarks. r^{2}SCAN-L additionally provides a pure KS treatment (hence enables a KS band-gap and optical excitation comparison with gKS results from r^{2}SCAN without the need for the OEP), and should, in most cases, support significantly faster solid calculations than r^{2}SCAN, on the timescale of an ordinary GGA. A further speedup of molecular calculations from r^{2}SCAN-L in a GTO basis will require addressing the remaining computational bottleneck, the calculation of $\nabla^2 n$ from GTO second derivatives on the integration grid (rather than directly as in a plane-wave code.) Nonetheless, calculations with r^{2}SCAN-L with the MEDIUM NWCHEM grid are as fast as those with SCAN with the XFINE grid.

Detailed molecular test-set results obtained with r^{2}SCAN and r^{2}SCAN-L, as well as the detailed results for the periodic solid test sets for all functionals, can be found in the Supplemental Material [32].

Acknowledgments. This work was supported by U.S. Department of Energy Energy Frontier Research Center Grant No. DE-SC 0019330.

[1] E. B. Isaacs and C. Wolverton, Phys. Rev. Materials **2**, 063801 (2018).
[2] J. Sun, A. Ruzsinszky, and J. P. Perdew, Phys. Rev. Lett. **115**, 036402 (2015).
[3] J. Sun, R. C. Remsing, Y. Zhang, Z. Sun, A. Ruzsinszky, H. Peng, Z. Yang, A. Paul, U. Waghmare, X. Wu, M. L. Klein, and J. P. Perdew, Nat. Chem. **8**, 831 (2016).
[4] J. G. Brandenburg, J. E. Bates, J. Sun, and J. P. Perdew, Phys. Rev. B **94**, 115144 (2016).
[5] N. Mardirossian and M. Head-Gordon, Mol. Phys. **115**, 2315 (2017).
[6] A. P. Bartók and J. R. Yates, J. Chem. Phys. **150**, 161101 (2019).
[7] D. Mejía-Rodríguez and S. B. Trickey, J. Chem. Phys. **151**, 207101 (2019)].
[8] H. Peng, Z.-H. Yang, J. P. Perdew, and J. Sun, Phys. Rev. X **6**, 041005 (2016).
[9] F. Tran, J. Stelzl, and P. Blaha, J. Chem. Phys. **144**, 204120 (2016).
[10] J. W. Furness, A. D. Kaplan, J. Ning, J. P. Perdew, and J. Sun, J. Phys. Chem. Lett. **11**, 8208 (2020).
[11] W. Kohn and L. Sham, Phys. Rev. **140**, A1133 (1965).
[12] M. Städele, J. A. Majewski, P. Vogl, and A. Görling, Phys. Rev. Lett. **79**, 2089 (1997)
[13] T. Grabo, T. Kreibich, and E. K. U. Gross, Molec. Eng. **7**, 27 (1997).
[14] T. Grabo, T. Kreibach, S. Kurth, and E. K. U. Gross, in *Strong Coulomb Correlations in Electronic Structure: Beyond the Local Density Approximation*, edited by V. I. Anisimov (Gordon and Breach, Tokyo, 2000), p. 203.
[15] A. Heßelmann and A. Görling, Chem. Phys. Lett. **455**, 110 (2008), and references therein.
[16] R. Neumann, R. H. Nobes, and N. C. Handy, Mol. Phys. **87**, 1 (1996).
[17] A. Seidl, A. Görling, P. Vogl, J. A. Majewski, and M. Levy, Phys. Rev. B **53**, 3764 (1996).
[18] Z. H. Yang, H. Peng, J. Sun, and J. P. Perdew, Phys. Rev. B **93**, 205205 (2016).
[19] J. P. Perdew, W. Yang, K. Burke, Z. Yang, E. K. U. Gross, M. Scheffler, G. E. Scuseria, T. M. Henderson, I. Y. Zhang, A. Ruzsinszky, H. Peng, J. Sun, E. Trushin, and A. Görling, Proc. Natl. Acad. Sci. USA **114**, 2801 (2017).
[20] D. Mejía-Rodríguez and S. B. Trickey, Phys. Rev. A **96**, 052512 (2017).
[21] D. Mejía-Rodríguez and S. B. Trickey, Phys. Rev. B **98**, 115161 (2018).
[22] F. Tran, P. Kovacs, L. Kalantari, G. K. H. Madsen, and P. Blaha, J. Chem. Phys. **149**, 144105 (2018).
[23] J. P. Perdew and L. A. Constantin, Phys. Rev. B **75**, 155109 (2007).
[24] A. C. Cancio and C. E. Wagner, arXiv:1308.3744.
[25] E. Aprà, E. J. Bylaska, W. A. de Jong, N. Govind, K. Kowalski, T. P. Straatsma, M. Valiev, H. J. J. van Dam, Y. Alexeev, J. Anchell, V. Anisimov, F. W. Aquino, R. Atta-Fynn, J. Autschbach, N. P. Bauman, J. C. Becca, D. E. Bernholdt, K. Bhaskaran-Nair, S. Bogatko, P. Borowski *et al.*, J. Chem. Phys. **152**, 184102 (2020)
[26] G. Kresse and J. Furthmüller, Phys. Rev. B **54**, 11169 (1996).
[27] G. Kresse and D. Joubert, Phys. Rev. B **59**, 1758 (1999).
[28] L. A. Curtiss, K. Raghavachari, P. C. Redfern, and J. A. Pople, J. Chem. Phys. **106**, 1063 (1997); L. A. Curtiss, P. C. Redfern, K. Raghavachari, and J. A. Pople, *ibid.* **114**, 108 (2001).
[29] V. N. Staroverov, G. E. Scuseria, J. Tao, and J. P. Perdew, J. Chem. Phys. **119**, 12129 (2003); **121**, 11507 (2004).
[30] J. P. Perdew, K. Burke, and M. Ernzerhof, Phys. Rev. Lett. **77**, 3865 (1996); **78**, 1396(E) (1997).
[31] D. Mejía-Rodríguez and S. B. Trickey, Phys. Rev. B **100**, 041113(R) (2019).
[32] See Supplemental Material at http://link.aps.org/supplemental/10.1103/PhysRevB.102.121109 for detailed molecular test-set results obtained with r^{2}SCAN and r^{2}SCAN-L, as well as the detailed results for the periodic solid test sets for all functionals.